Observation of the complete rupture of a buried polymer layer by off-specular neutron reflectometry

J. P. de Silva[1] [(a)(b)], S. J. Martin[1] [(c)], R. Cubitt[2] and M. Geoghegan[1]

[1] *Department of Physics and Astronomy, University of Sheffield, Hounsfield Road, Sheffield S3 7RH, U. K.*
[2] *Institut Laue-Langevin, 6 rue Jules Horowitz, BP 156, F-38042 Grenoble Cédex, France*

PACS `61.12.Ha` – Neutron reflectometry
PACS `68.05.-n` – Liquid-liquid interfaces
PACS `68.47.Mn` – Polymer surfaces

Abstract. - We have used off-specular neutron reflectometry to study the rupture of a thin, deuterated polystyrene layer confined between a silicon substrate and a thick poly(methyl methacrylate) upper layer. After total rupture of the buried layer the resulting roughness at the interface that controls the the total reflection edge gives rise to Yoneda off-specular scattering. This hypothesis is confirmed by specular reflectivity data that can be fitted to an effective error function subsequent to the rupture of the buried layer. The observed increase in the Yoneda peak intensities, integrated along the path of constant momentum transfer q_z, can be directly related to the formation of an interdigitated structure upon rupture of the buried layer. A distorted-wave Born approximation is used to quantitatively simulate the form of the off-specular data in terms of an equivalent error function, with fitting parameters in good agreement with the physical properties of the samples and key experimental results.

Introduction. – The stability of a polymer film depends on the surrounding medium as well as its substrate. It is thus possible that a normally stable film will dewet if thin enough and if covered by a medium whose attractive van der Waals interaction with the substrate exceeds its own such interaction. Although the stability of polymer films is a mature subject with many experiments performed [1,2], there is still much that is not studied or not understood. A particularly interesting area that has been little considered is the dewetting of the buried layer in a polymer bilayer. Here the interest is because the stability can be readily controlled by altering the thickness of both layers [3]. The study of the interface between two polymer layers can be readily achieved by the use of a selective solvent to dissolve the upper layer to reveal the morphology of the interface. This has been achieved with the polystyrene-poly(methyl methacrylate) (PMMA) system that we study here. Most of the bilayer experiments have used cyclohexane to dissolve an upper layer of polystyrene, allowing the buried interface with PMMA to be studied by scanning force microscopy (SFM) [1]. Not only are such SFM experiments inherently destructive, it is possible that the acid rinse will also interfere with the interface of interest. A polymer-polymer interface consists of interdigitated chains, as well as thickness fluctuations (capillary waves). The buried layer of thickness L can be described by a thickness dependent free energy function W, given by

$$W(L) = -\frac{A_{123}}{12\pi L^2} - \frac{A_{1234}}{12\pi (L+h)^2}, \qquad (1)$$

where A_{123} and A_{1234} are the respective Hamaker constants describing the interaction between the top polymer layer of thickness h and the substrate, and the interaction between the ambient environment (usually air, nitrogen, or vacuum) and the substrate across the polymeric bilayer; the subscripts 1-4 correspond to the substrate, buried polymer layer, upper polymer layer, and ambient environment respectively. Such a layer may be unstable if $d^2W/dL^2 < 0$ and may dewet with a preferred length-scale Λ predicted by $\Lambda = \left[-4\pi^2\gamma/(d^2W/dL^2)\right]^{1/2}$, where γ is the interfacial energy of the buried, highly deformable liquid-liquid interface [4,5].

[(a)]E-mail: `j.desilva@physics.org`
[(b)]Present address: Laboratoire de Physique des Solides, UMR 8502 Université Paris Sud, F-91405 Orsay, France
[(c)]Present address: Department of Materials, Loughborough University, Leicestershire LE11 3TU, U. K.

Neutron reflectometry is an ideal tool to study the interface between two polymer layers [6], and experiments using off-specular reflectivity are capable of revealing information about lateral structure [7] as well as the more usual depth profile. However, off-specular measurements such as those that rely on Bragg-type scattering require long acquisition times depending on the degree of lateral ordering. Here we show (specular) neutron reflection data that reveal information about the laterally averaged shape of the interface as a function of depth from the substrate, as well as off-specular data that reveal the point at which the buried film ruptures. We use the onset of off-specular Yoneda scattering, which is due to non-correlated roughness, in order to better understand the structure formation at buried interfaces; a consequential advantage is that much lower acquisition times are required in order to collect representative data.

Experimental. – Thin, monodisperse deuterated polystyrene (dPS) (217 kDa) films of 3, 7, 11, 15, and 30 nm thick were spin coated onto 5 cm silicon substrates. Monodisperse PMMA (281 kDa) was spun cast onto cleaved mica to form a film of 205±5 nm. The PMMA film was floated onto deionized water and picked up onto the polystyrene film on the silicon wafer to create a bilayer structure. The resultant bilayers were dried under vacuum at 333 K for 2 h in order to remove residual water. These bilayers were annealed at 423 K for 0.5, 1, and 2 h and 433 K and for 3 and 8 h. In the case of this model system, γ=1.52 mJm^{-2} at 433 K (the calculated, temperature dependent dPS-PMMA interfacial tension) and $A_{123} > 0, A_{1234} < 0$ for the chosen experimental thickness range, ultimately driving an instability in the buried dPS layer when annealed above the T_g of both polymers [3], where $\Lambda \approx 1\,\mu$m (confirmed by SFM measurements). Scattering length densities (SLDs) for PMMA, dPS and Si are taken as 1.07, 6.48 and 2.08×10^{-6} Å^{-2} respectively. The amorphous silicon oxide layer is neglected when fitting the data, and the substrate roughness is invariant at 0.5 nm.

Neutron reflection experiments were performed using the time-of-flight reflectometer D17 at the Institut Laue Langevin. The D17 reflectometer incorporates a high-resolution area detector that permits the concurrent capture of both specular and off-specular scattering data. The spectrometer is used in time-of-flight (TOF) mode with a relaxed momentum transfer ($\hbar q$) resolution in order to maximize the data acquisition rate. Off-specular scattering is orders of magnitude weaker than the specular reflection, and therefore the acquisition times required for convincing statistics are far greater. Data are collected for two angles covering a q_z range of 0.008 to 0.24 Å^{-1}. Specular data over the whole q_z range are analysed using downhill simplex routines to fit a model profile to the reflectivity data [8] by minimisation of χ^2 on normalised data combined from both angles at an appropriate value of q_z. Normalised off-specular data are manipulated using the LAMP [9] software.
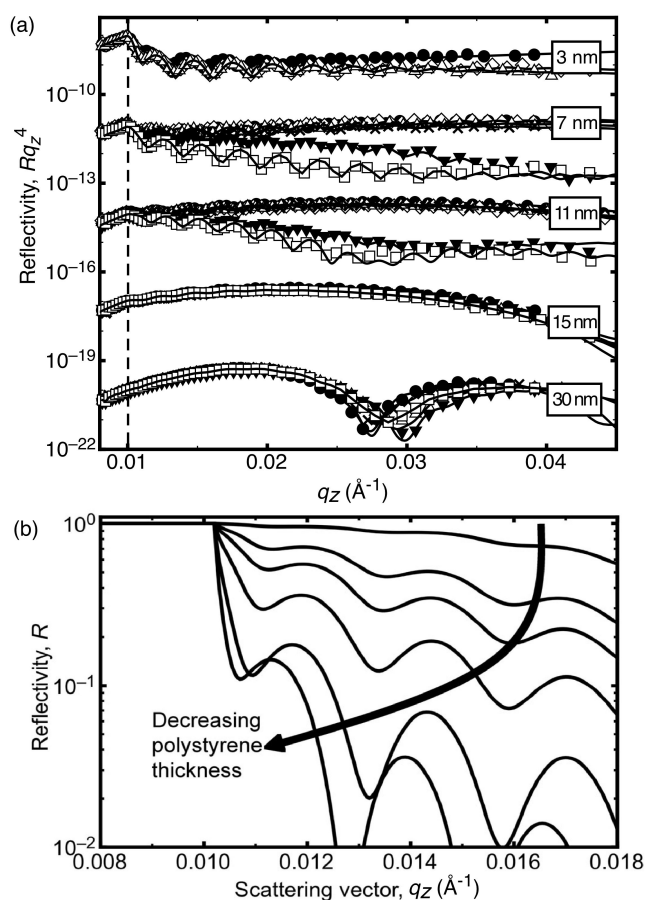

Fig. 1: (a) Smaller angle specular reflectivity data $Rq_z^4(q_z)$ and fits for all sample sets annealed for 0 (●), 0.5 (◇), 1 (△), 2 (×), 3 (▼) and 8h (□). Each dataset is offset by 10^{-3} for clarity, the total reflection edge is marked by the dashed line.(b) Simulated reflectivity $R(q_z)$ around the total reflection edge for a 210 nm PMMA film on deuterated polystyrene films of thickness 30, 15, 11, 7, 3, and 0 nm, the latter being a single PMMA layer.

Results and discussion. – Specular reflectivity data in the form $Rq_z^4(q_z)$ for all dPS thicknesses are shown in fig. 1(a) for a set of bilayers annealed for different times. Fits to all of the data are of good quality, with typically $\chi^2 < 2$. It is interesting to note that fringes remain visible for the polystyrene layer in the reflectivity curves for the thicker polystyrene layers, which is an indication of the integrity of this layer. When these fringes disappear, the Kiessig fringes for the whole bilayer remain (although difficult to determine in these plots), but the reflectivity decreases. This can be confirmed by simulated reflectivities shown in fig. 2(b), where the resolution is 0.01% of q_z,

the roughnesses and interfacial widths are all 0.01 nm, and incoherent terms in the scattering length densities were set to zero in order to show the total reflection edge without being affected by other phenomena. Increasing the polystyrene thickness has the effect of starting to move the total reflection edge. This is an indication, not only
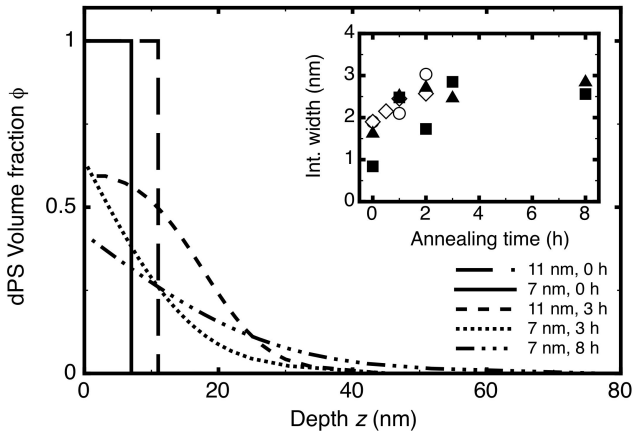
Fig. 2: Example of effective dPS volume fraction profiles, corresponding to unannealed and post-rupture samples where the data are well fitted to an error function profile. (*Inset*) Polymer-polymer interfacial widths for all samples prior to the total rupture of the buried layer for dPS thicknesses 7 ($\circ$), 11 ($\diamond$), 15 ($\blacktriangle$) and 30 nm ($\blacksquare$).

of an increase in the transmission of neutrons through the film, but of off-specular scattering. The PMMA surface roughness plays a limited role in the fitting of the data, supporting the premise that the experiment specifically targets the buried layer. The strong reduction in reflectivity after 0.5, 2 and 3 h annealing for the 3, 7 and 11 nm dPS samples respectively is attributed to the complete rupture of the buried dPS layer. It is no longer possible to fit the data to a slab model after this point, and subsequently the complementary error function model describes the data well, while preserving the total volume of dPS material.

For films that had not undergone complete rupture, a bilayer profile was appropriate, consisting of two step functions convolved with a Gaussian roughness function. For films in which the PMMA layer penetrated the polystyrene layer to the substrate, the volume fraction, ϕ of deuterated polystyrene decreases to zero with distance, z from the substrate in a manner that could be effectively fitted with a complementary error function profile of the form

$$\phi(z) = \phi_0 + (\phi_1 - \phi_0)\frac{\mathrm{erfc}\,(z - \Delta z/w)}{\mathrm{erfc}\,(\Delta z/w)}, \qquad (2)$$

where ϕ_1 is the areal average polystyrene volume fraction at the surface, $\phi_0 = 0$ is the volume fraction away from the substrate, Δz is an offset, and w is the width of the complementary error function. When Δz is equal to the thickness of the original polystyrene layer, $\phi_1 = 1$.

The error functions shown in fig. 2(a) give some indication as to the lateral dimensions of the interdigitated structure that is formed by the rupture of the buried layer. It should be noted that such an error function may be used here to describe an *immiscible* system because the coherence length of the neutrons is greater than the structural

length scales of around 1 μm, so the neutrons interact with a SLD averaged over the different phases. The interfacial widths for the 3, 7 and 11 nm samples continue to increase up to the point of rupture, as expected for such unstable buried layers, while on the timescale of the experiment the 15 and 30 nm samples are rather stable and thus tend towards an equilibrium interfacial width that can be predicted by considering the capillary fluctuations sustainable by the liquid-liquid interface [10]. (The surface of the PMMA remains relatively uniform over the time period of these experiments, limiting any contribution from its dewetting—spontaneous or otherwise—to the processes observed here.) The observed late stage interfacial widths for the 15 and 30 nm samples are indeed in good agreement with a theoretically calculated value of approximately 2.4 nm for these polymers and temperatures [10]. Such values are also in good agreement with SFM data for both interfaces before and after the selective dissolution of the PMMA capping layer using acetic acid as a selective solvent.

In fig. 3 we show an example of off-specular data for pre- and post-ruptured samples, presented as neutron wavelength λ against $2\theta/2$, where the scattering angle $2\theta = (\alpha_i + \alpha_f)$, α_i and α_f are the angles of the incident and scattered waves respectively, and larger values of wavelength correspond to slower neutrons and thus smaller q_z. The refracted transmission peak is barely visible at the far left hand side, the longest vertical line to the right of the transmission is the specular reflectivity defined by $2\theta = 2\alpha_i$. The detector is placed 3.4 m from the sample centred at an angle of $2\theta = 2.5°$; it is clear from fig. 3 that the specular reflection is placed off-centre in order to give access to an increased q_x range. Correlated, off-specular Bragg scattering from approximately one micron dewetted structures should be manifested as visible peaks of around $q_x = 6.3 \times 10^{-4}$ Å^{-1} for the first order (discussed in detail below), but any firm indication of this is not systematically observed. The absence of off-specular Bragg scattering may be due to two possibilities: the periodicity of the dewetted buried structure may not be strong enough to give rise to the off-specular reflection, or the peaks may be there, but so weak that they are lost in experimental noise. Certainly, one of the few experiments so far to realise off-specular Bragg scattering is that due to Sferrazza and co-workers [7], who were only able to achieve the identification of off-specular Bragg scattering by using a constant wavelength and collecting large statistics on the shoulder of the specular scattering peak. The TOF experiment employed here is not suited to an analysis based on Bragg diffraction due to the rather low off-specular intensities acquired.

Despite off-specular Bragg scattering not being detected, we note the existence of Yoneda peaks [11] that trace a path from the specular total reflection edge to the horizon ($2\theta = \alpha_i$), as highlighted in fig. 3. Yoneda scattering occurs when radiation is incident on a surface of higher refractive index than the medium in which it is initially
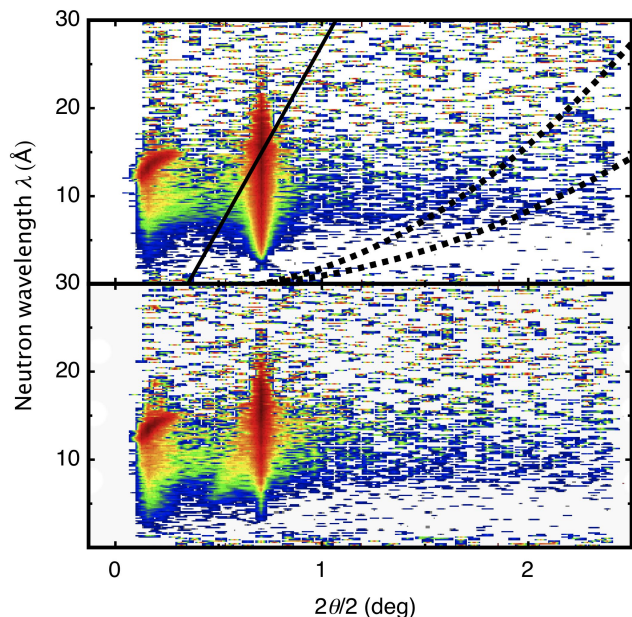
Fig. 3: Plot showing off-specular neutron data (intensity is presented logarithmically) for an 11 nm dPS sample (*top*) unannealed and (*bottom*) annealed for 8 h. The solid line defines $q_z = 0.0105$ Å^{-1} (corresponding to the critical angle) which intersects the specular at the total reflection edge, the expected path traced by the Yoneda peak. The dashed lines are the representative positions of first and second order Bragg peaks due to a one micron lateral structure, $q_x = 6.3$ and 12.6×10^{-4} Å^{-1} respectively.

travelling, and is observed when either the incident or exit angles are equal to the total reflection angles for that wavelength. In the case of the incident angle equalling θ_c, the refracted wave is in the plane of the interface and may be scattered out of the film by roughness in the sample. The scattered radiation must exit the sample at an angle greater than θ_c. In the case of the exit angle equalling θ_c, the path of the radiation is the reverse of that for the case of the incident angle equalling θ_c, since the direction of radiation must be reversible. In our case, the exit angle is equal to θ_c and it is therefore interfacial roughness that causes an incident wave that one would normally expect to be (mostly) transmitted to be refracted into the plane of the surface.

The onset of Yoneda scattering in the 3, 7 and 11 nm data corresponds to the complete rupture of the buried dPS layer. This is because there can be no change in neutron contrast at the solid Si interface until rupture of the buried layer occurs. We find that the intensity of the Yoneda peak on the horizon side of the specular reflectivity is of much higher magnitude, indeed a Yoneda peak to the right of the specular reflection is never observed in our samples due to this disparity. Due to the nature of TOF data, all wavelengths up to the critical wavelength ($\lambda \approx 14$ Å) contribute to the Yoneda peak on the horizon side of the specular reflection (satisfied by $\alpha_f = \theta_c$),

whereas on the reverse side only a single incident wavelength contributes ($\alpha_i = \theta_c$) resulting in a disparity in intensity possibly of one or two orders of magnitude. In the subsequent analysis we therefore neglect the Yoneda peak on the non-horizon side of the specular reflection.

The Yoneda peak is not evident in any of the samples prior to annealing, so there is a point at which the roughening of the interfaces becomes significant enough to cause the resulting Yoneda scattering. Simulations show that the total reflection edge is controlled by the silicon-dPS interface up to 30 nm thickness of dPS, as shown in fig. 1(b). This means that any visible Yoneda peaks should always converge to the Si critical edge. In order for the Yoneda peaks to be observed the sample must have sufficient roughness at the critical edge to cause strong diffuse scattering. As the silicon-dPS interface is non-deformable, we interpret the onset of Yoneda peaks as the point at which the buried deuterated polystyrene film completely ruptures and the PMMA makes contact with the Si surface, creating a high contrast rough interface giving rise to diffuse scattering. In the case of the thin polystyrene films, the deuteration is not enough to move the total reflection edge to higher values of q_z; for this reason, the total reflection edge for all rupturing samples (3 to 11 nm) is located at $q_z = 0.0105$ Å^{-1}, the value for silicon. When the PMMA makes contact with the substrate, the roughness gives rise to the Yoneda peaks.

We present in fig. 4 the integrated off-specular intensity of the Yoneda peak versus annealing time for all sample sets, together with the associated PMMA volume fraction at the Si interface after rupture. We use a novel approach to analyse the rather weak Yoneda peaks: the total intensity is derived by integrating along the path defined by $q_z = 0.0105$ Å^{-1} (as indicated in fig. 3), which corresponds to the wavelength dependent path traced by the Yoneda peak at a constant momentum transfer defined by the critical angle, and in this way the result is optimised to exclude any diffuse broadening of the specular reflectivity and other artefacts. The intensities are normalised to the unannealed samples. We see that the strong asymptotic increase in Yoneda intensity corroborates the expected point of rupture for the 3, 7 and 11 nm samples as determined by the specular reflectivity data. The 7 and 11 nm samples in particular show the clearest indication, with intensities around unity (*i.e.* no change from the unannealed samples) until 2 and 3 h annealing respectively, where the Yoneda scattering increases sharply as the buried layer ruptures. One may expect it to be possible to relate the intensity of the Yoneda to the contrast generated by the form of the buried structure: we see in fig. 4 for instance that the Yoneda intensity reaches a maximum after 3 h annealing, but subsequently falls after 8 h annealing. This may be due to the PMMA becoming the majority material at the Si interface (when $(1 - \phi) > 0.5$) and thus the effective SLD contrast is actually reduced. This may also indicate some large-scale structural evolu-
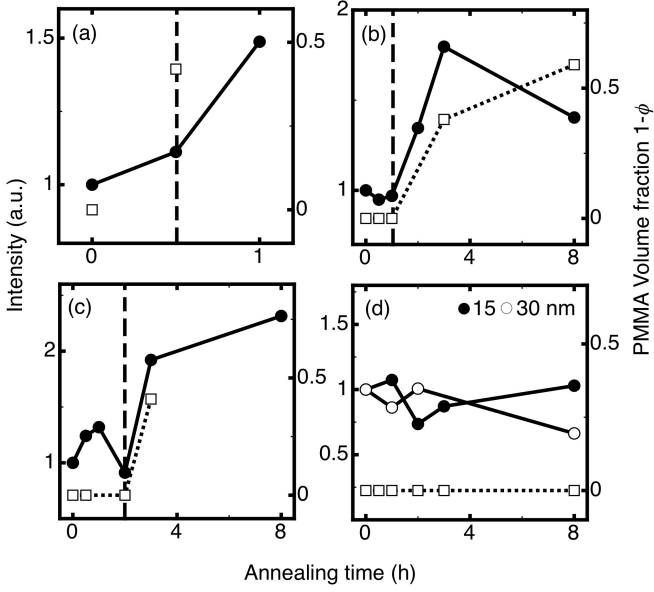
Fig. 4: Normalised, integrated Yoneda intensity (●) and effective PMMA volume fraction at the Si interface (□) against annealing time, for dPS thicknesses of 4 (a), 7 (b), 11 (c), and 15 and 30 nm (d). Dashed vertical lines correspond to the point of complete rupture of the buried dPS layer.

tion, such as the onset of layer inversion due to the formation of a wetting layer of PMMA at the Si interface for instance [12]. The intensity of the Yoneda scattering relative to the unannealed sample also increases with increasing dPS thickness (more deuterated polymer causing more scattering), ranging from a factor of 1.5 for the 3 nm sample up to 2.3 times the intensity of the unannealed sample for the 11 nm dPS sample. There may be some evidence of early Yoneda scattering in the unannealed 3 nm sample, possibly due to partial dewetting of the 3 nm thick dPS layer during sample preparation.

The thicker 15 and 30 nm samples do not exhibit a well defined Yoneda peak at any stage of annealing because the buried layers do not proceed to complete rupture, either due to the time scale of the experiment being shorter than that of the rupture timescale, or simply that the buried layers are stable in this configuration. Certainly we do not see in fig. 4 any clear change in Yoneda intensity for these sample sets. Symmetric lateral broadening of the specular peak in the thicker dPS samples is indicative of increased diffuse scattering, possibly from the roughening dPS-PMMA and PMMA-air interfaces, as confirmed by the interfacial widths derived from the specular data. As shown in fig. 3 it is possible that the total reflection edge shifts towards the polymer-polymer interface for the 30 nm sample, and thus the increase in diffuse scattering seen in these samples may be attributed to the polymer-polymer interface as there is no rough structure at the Si interface. There is some evidence of scattering due to a correlated roughness as seen to the left of the specular peak in fig. 3 for instance, this may be related to increased neutron

statistics from the thicker dPS layer or strong scattering from the polymer-polymer interface.

In order to form a quantitative description of the off-specular data and confirm that features such as the Yoneda peak are correctly interpreted, we perform simulations of the off-specular intensity using parameters that relate to the physical structure of the studied system. The form of the off-specular reflectivity may be described by a modified form of the distorted-wave Born approximation (DWBA) [13,14], where the diffuse intensity I_d is given by

$$
I_d = I_0 \left| T_i T_f (1 - n^2) \exp\left(-(q_z^t)^2 \frac{\Sigma^2}{2} \right) \right|^2
$$
$$
\frac{\exp\left(-\left[(q_z^t)^2 + (q_z^{t*})^2 \right] \sigma^2 / 2 \right)}{|q_z^t|^2}
$$
$$
\int_{-\infty}^{\infty} \left(\exp\left(|q_z^t|^2 \sigma^2 \exp\left[-\left| \frac{X}{\xi} \right|^{2H} \right] \right) - 1 \right) \cos(q_x X) \mathrm{d}X,
$$

(3)

where I_0 is a constant, and (adhering to the notation of Sinha et al. [13]) q_z^t is the momentum transfer inside the medium, T_i and T_f are the Fresnel transmission functions of the incident and scattered waves, the neutron refractive index $n = 1 - (\lambda^2 \rho / 2\pi) + i(\lambda \mu / 4\pi)$ where ρ is the SLD difference at the scattering interface and the absorption coefficient μ is taken to be 10 % of ρ, Σ is the width of an error function that simulates an SLD gradient across the rough interface, σ is the physical roughness of the interface in question, X is the distance between any two points on the simulated fractal surface, ξ is a cut-off in the correlation length of the fractal surface, and H is the Hurst parameter that describes the nature of the fractal surface, varied between zero and unity, the latter corresponding to a less chaotic, more self-affine roughness. As the data are TOF we must consider that multiple λ contribute to any single value of 2θ; we therefore simulate q_x and q_z terms λ using the relations $\lambda = 2\pi \sin(2\theta)/q_z$ and $\lambda = 2\pi \left[\cos(2\theta - \alpha_i) - \cos(\alpha_i) \right]/q_x$ [15]. As the majority of the fitting parameters fall within an integral with a non-analytical solution, simulations are performed by solving numerically for any chosen fit parameters. Such a model superimposes an error function profile across the rough interface, which allows for a consistent model with the previously determined specular reflectivity profiles, but with an important caveat: here we consider only the refractive index difference at a single interface rather than the true bilayer model as used to fit the specular reflectivity data.

We present in fig. 5 DWBA simulations of diffuse intensity corresponding to horizontal slices of $\lambda = 8, 11$ and 15 Å through the experimental data shown in fig. 3 for the fully ruptured 11 nm sample. For $2\theta < \alpha_i$ we are in the medium and the transmission function is essentially imaginary. The simulation is performed using parameters $H = 0.3$, $\rho = 5.4 \times 10^{-6} \, \text{Å}^{-2}$, $\sigma = 3.2 \, \text{nm}$, $\Sigma = 11.5 \, \text{nm}$ and $\xi = 32000 \, \text{nm}$. We see that the prominent features are

reproduced, including the diffuse width of the specular reflection peak, the strong decrease in specular reflectivity with increasing q_z, the ratio of the Yoneda peak to that of the specular peak and finally the position of the Yoneda peaks, which are not so clearly delineated by eye in the experimental data due to scatter in the data but can be more clearly determined from fig. 3. The values of σ and Σ correspond well to those derived from the specular reflectivity fits shown previously: although the value of Σ is around a quarter of that used above to fit the specular reflectivity data, this can be clearly attributed to the prior discussed simplifications of the diffuse model. Here we interpret the rather large cut-off length ξ to be a consequence of the beam averaging the interface over length scales much larger than the rupture length scale; such large cut-off lengths have been reported previously for off-specular neutron reflectivity data [17]. While this simple model reproduces the main features of the off-specular data rather well, improved statistics and convolution of the simulation with a resolution function will permit further refinement.
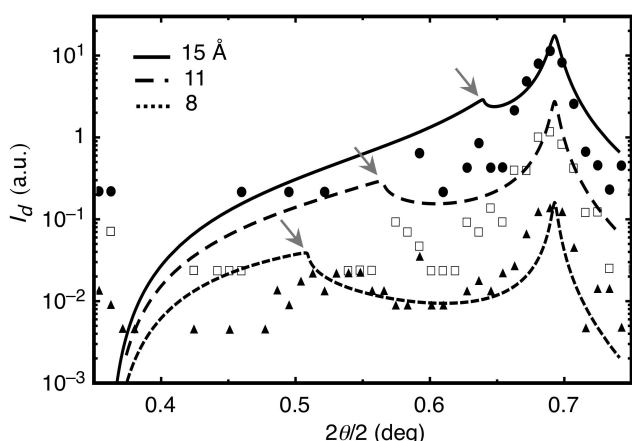

Fig. 5: Simulations of off-specular intensity I_d for $\lambda = 8, 11$ and 15 Å and corresponding experimental data for the 11 nm dPS sample after 8 h annealing for $\lambda = 8$ (▲), 11 (□) and 15 (●) Å. (Yoneda peaks arrowed.)

Conclusion. – We have performed neutron reflectometry experiments to demonstrate the rupture of a buried polymer bilayer. Specular neutron reflectometry probes the transition from a simple bilayer structure to one where the volume fraction profile can be characterised by an error function, while off-specular neutron reflectometry is used to demonstrate that the rupture of the buried polymer layer can be revealed by the appearance of Yoneda scattering. We show that the onset of strong diffuse scattering and Yoneda peaks can be quantitively predicted by DWBA simulations that confirm the experimental observations. This off-specular scattering convincingly demonstrates that the film has ruptured, without the ambiguity associated with an error function profile, which may also indicate a laterally homogeneous structure. Although

Yoneda peaks are readily studied in X-ray scattering [16], their usage in neutron reflection from polymeric materials is thus far limited to observing roughness [18] for instance. It is hoped that these results will encourage further study into the practical and quantitative application of off-specular neutron scattering to the determination of buried structures.

REFERENCES

[1] GEOGHEGAN M. and KRAUSCH G., *Prog. Polym. Sci.*, **28** (2003) 261.
[2] MÜLLER-BUSCHBAUM P., *J. Phys.: Condens. Matter*, **15** (2003) R1549.
[3] DE SILVA J. P., GEOGHEGAN M., HIGGINS A. M., KRAUSCH G., ODILE M.-O. and REITER G., *Phys. Rev. Lett.*, **98** (2007) 267802.
[4] VRIJ A., *Discuss. Faraday Soc.*, **42** (1966) 23.
[5] BROCHARD-WYART F., MARTIN P. and REDON C., *Langmuir*, **9** (1993) 3682.
[6] RUSSELL T. P., *Mater. Sci. Rep.*, **5** (1990) 171.
[7] SFERRAZZA M., HEPPENSTALL-BUTLER M., CUBITT R., BUCKNALL D. G., WEBSTER J. and JONES R. A. L., *Phys. Rev. Lett.*, **81** (1998) 5173.
[8] JONES R. A. L., NORTON L. J., SHULL K. R., KRAMER E. J., FELCHER G. P., KARIM A. and FETTERS L. J., *Macromolecules*, **25** (1992) 2359.
[9] LAMP, the Large Array Manipulation Program (http://wwwold.ill.fr/data_treat/lamp/lamp.html)
[10] SFERRAZZA M., XIAO C., JONES R. A. L., BUCKNALL D. G., WEBSTER, J. and PENFOLD, J., *Phys. Rev. Lett.*, **78** (1997) 3693.
[11] YONEDA Y., *Phys. Rev.*, **131** (1963) 2010.
[12] STEINER U., KLEIN J. and FETTERS L. J., *Phys. Rev. Lett.*, **72** (1994) 1498
[13] SINHA S. K., SIROTA E. B., GAROFF S. and STANLEY H. B., *Phys. Rev. B*, **38** (1988) 2297
[14] WORMINGTON M., PAPE I., HASE T. P. A., TANNER B. K. and BOWEN D. K., *Phil. Mag. Lett.*, **74** (1996) 211.
[15] SALDITT T., MÜNSTER C., MENNICKE U., OLLINGER C. and FRAGNETO, G., *Langmuir*, **19** (2003) 7703.
[16] WOLKENHAUER M., BUMBU G.G., CHENG Y., ROTH S. V., and GUTMANN J. S., *Appl. Phys. Lett.*, **89** (2006) 054101.
[17] LAVERY K. A., PRABHU V. M., LIN E. K., WU W., SATIJA S. K., CHOI K.-W. and WORMINGTON M., *Appl. Phys. Lett.*, **92** (2008) 064196.
[18] WANG W., METWALLI E., PERLICH J., TROLL K., PAPADAKIS C. M., CUBITT R. AND MÜLLER-BUSCHBAUM, P., *Macromol. Rapid Commun.*, **30** (2009) 114.